Effect of fracture behavior variables on hydraulic fracturing optimization by adding graphene nanosheets to sand/water mixtures: A molecular dynamics approach

Wei Zhu [a], Farahnaz Saberi [b], S. Mohammad Sajadi [c], Navid Nasajpour-Esfahani [d], Maboud Hekmatifar [e], As'ad Alizadeh [f,*], D. Toghraie [e,*], Roozbeh Sabetvand [g]

[a] School of Resources and Safety Engineering, Central South University, Changsha 410083, China
[b] Institute of Petroleum Engineering, Department of Chemical Engineering, College of Engineering, University of Tehran, Tehran, Iran
[c] Department of Nutrition, Cihan University-Erbil, Kurdistan Region, Iraq
[d] Department of Material Science and Engineering, Georgia Institute of Technology, Atlanta 30332, USA
[e] Department of Mechanical Engineering, Khomeinishahr Branch, Islamic Azad University, Khomeinishahr, Iran
[f] Department of Mechanical Engineering, College of Engineering, Urmia University, Urmia, Iran
[g] Department of Energy Engineering and Physics, Faculty of Condensed Matter Physics, Amirkabir University of Technology, Tehran, Iran

ARTICLE INFO

ABSTRACT

Hydraulic fracture is one of the promising techniques for the breakage of rock without blasting, thus the investigation of its internal mechanism is helpful to develop forecasting system for ground pressure. In this study, molecular dynamics (MD) method was used to describe the effect of graphene nanosheets (GNS) (with different edges) on the hydraulic fracturing process. More specifically, in the MD box, we simulated the effects of GNS on rock substrates, the mixtures of H_2O and sand, and sands that deviate from the specified atomic substrates. Therefore, we calculated the parameters, such as temperature, total energy and mutual forces of atomic structures. In these simulations, mixture fluid is simulated by sand particles and water molecules with the Universal Force Field (UFF). Physically, adding GNS to mixture fluid caused a decrease in the number of trapped sand particles in the fracture of rock matrix. The sand particles removed from rock matrix fracture. This atomic phenomenon optimized the hydraulic fracturing process and reduced operating costs. Numerically, in our simulations, the atomic structures' temperature and potential energy converged to 300 K, and −479 eV (respectively). Furthermore, trapped sand particles in MD simulations decreased to 14 particles using GNS. Our results show that the trapped sand particles reached their minimum rate (14 particles) by 2.5% atomic ratio of GNS inserting into the initial atomic mixture fluid. This atomic behavior results from the energy of the interactions between sand particles, and rock substrate. The interaction energy between the sand particles and the substrate reduced to a −32.38 eV by adding GNS to original H_2O-sand mixture. This atomic evolution caused the volume of trapped sand particles reached to minimum value in the presence of GNS with optimum atomic ratio.

1. Introduction

The hydraulic fracturing process is a drilling technique used to extract natural gas or oil from deep underground (see Fig. 1). However, it is an economical and safe source of clean energy; critics claim that the hydraulic fracturing process can pollute air, and trigger earthquakes [1]. The hydraulic fracturing procedure started in recent decades, and the first useful usage was in 1950. Numerically, 2.5 million professions were created in the oil industry in the world, and only about 1.000.000 of these jobs in the USA were formed [2,3]. This process is essential to gain enough flow rates in tight gas, shale gas, coal seam gas wells, and tight oil [4,5]. Sometimes hydraulic fractures create in dykes or certain veins [6]. America became a leading crude oil exporter through hydraulic fracturing in recent years [7], but methane, a greenhouse gas, increased during this procedure [8]. Increasing fossil fuels produced from the decade led to a lower cost of consumption for humans [9,10]. Practically, we can decrease the environmental population of this procedure (by reducing oil extraction volume).
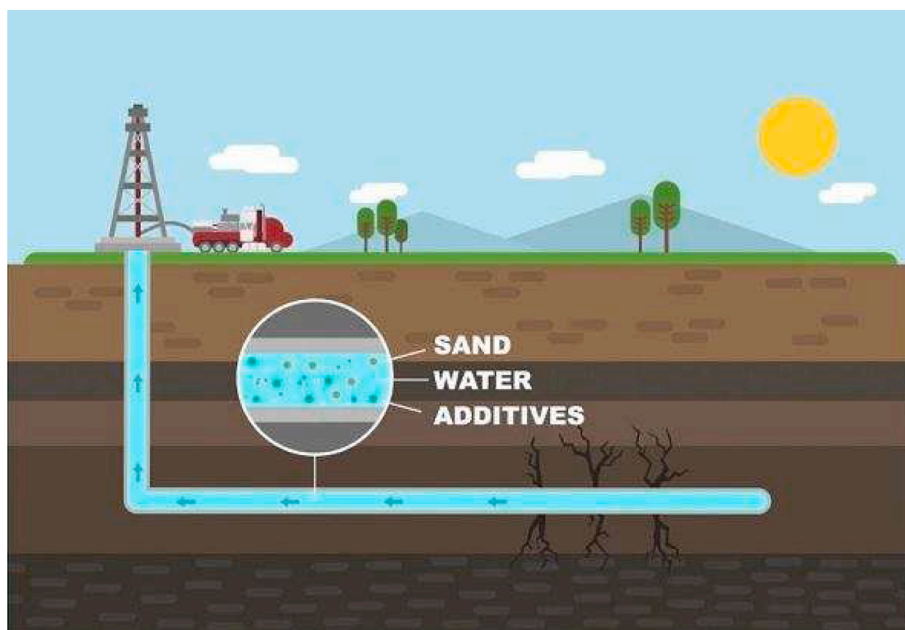
Fig. 1. A Schemaice of the hydraulic fracturing procedure.
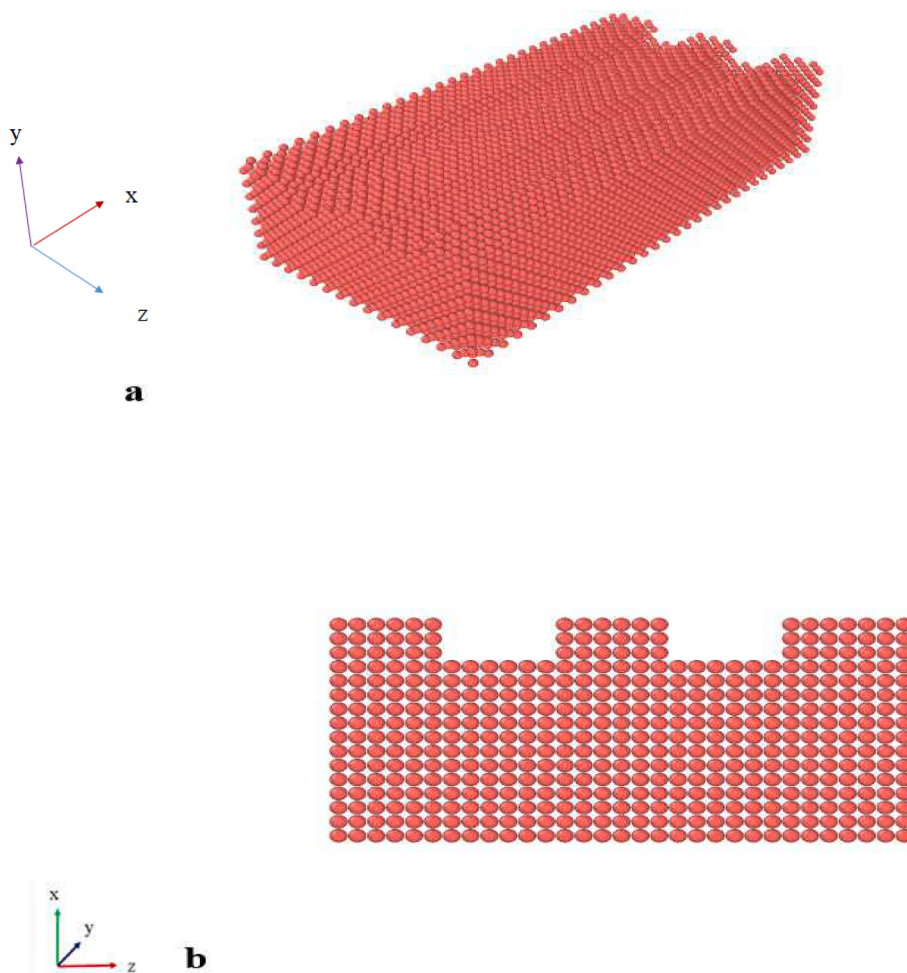
Fig. 2. Schematic of rock substrate with a fracture at a) Perspective and b) front views.
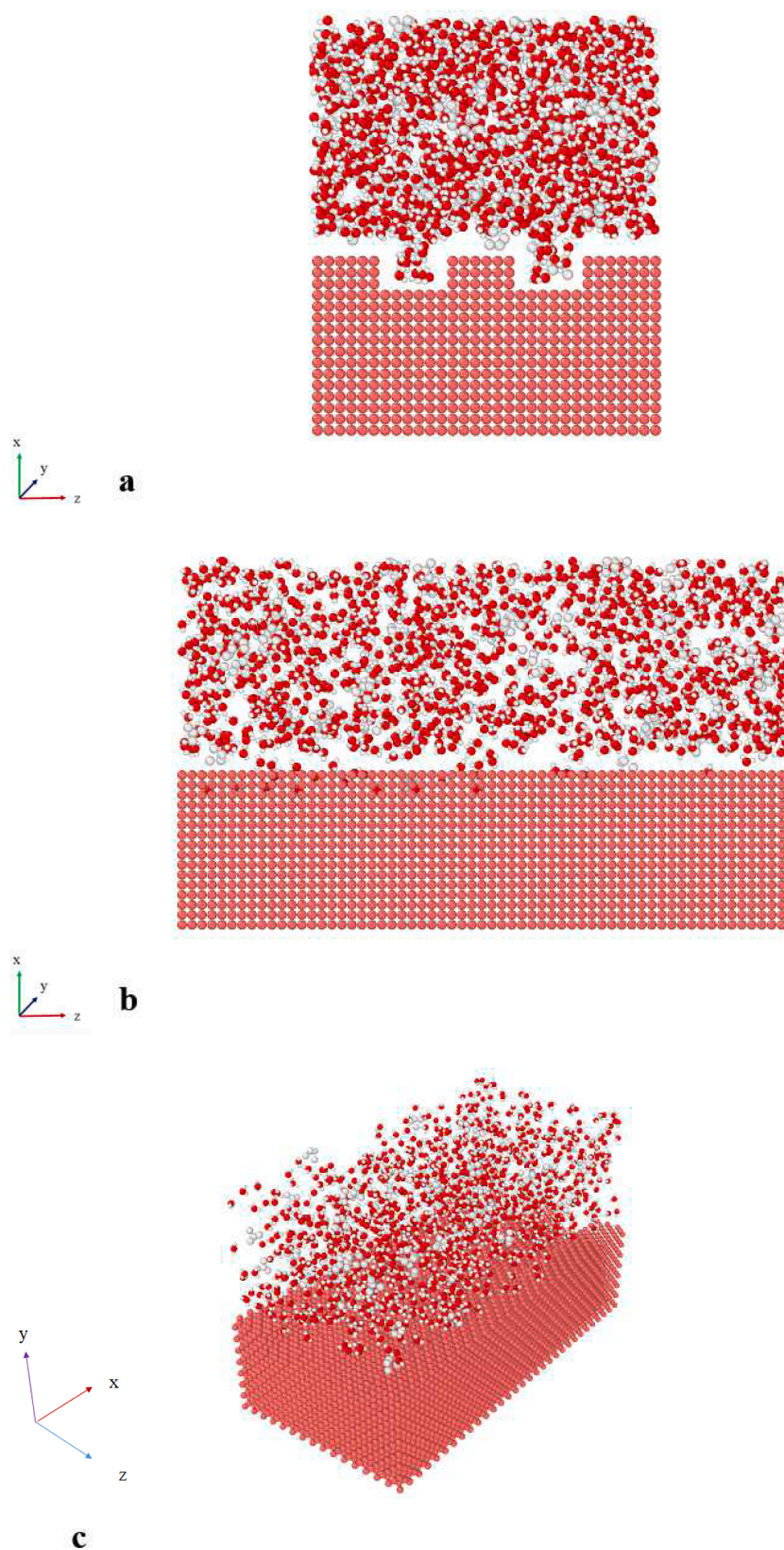
Fig. 3. Schematic of rock substrate and H_2O-sand mixture is depicted by OVITO software at a) Front, b) Top, and c) Perspective views.

Table 1
The ε_{ij} and σ_{ij} for Lennard-Jones interaction in this MD study [35].

Atom	ε_{ij} (kcal/mol)	σ_{ij} (Å)
O	0.060	3.500
Si	0.402	4.295
Al	0.505	4.499
Fe	0.013	2.912
Ca	0.238	3.399
Na	0.030	2.983
P	0.305	4.147
Mg	0.111	3.021

Table 2
MD simulation details in current computational research.

Computational Parameter	Simulation Settings
Computational Box Length	$100 \times 50 \times 75$ Å³
Boundary Condition	Periodic Boundary Condition
Simulation Algorithms	NVT/NVE
Initial Temperature	300 K
Time Step	1 fs
Damping Ratio for Temperature	0.01
Total Simulation Time	5 ns

The hydraulic fracturing process has many adverse environmental effects on the environment and human society [11,12]. Wigwe et al. [13] studied the effect of fraction densities, injection rates, fluid viscosities. Jahandideh et al. [14] and Cao et al. [15] investigated the optimization of the hydraulic fracturing design that affected economic problems. Nanotechnology is one of the choices to affect optimizing the hydraulic fracturing method. In other words, nanotechnology is engineering and science, technology managed at the nanoscale, which was about 1 to 100 nm and we used nanostructures, such as graphene, carbon nanotube, etc., in different area [16–18]. Finally, environmental population declined as a result of this process (by decreasing the rate of oil extraction). GNS is one of the most promising nanotechnology structures. This atomic structure is an allotrope of carbon in a single layer of atoms [19]. Recently, this nanometric structure was used in the

petroleum industry for optimizing various industrial aims. Sepehri et al. [20] showed the graphene nanostructure could be used as remarkable material for revolution in the petroleum industry. This research showed the appropriate graphene function in drilling, desalination, cementing, and cleaning oil spills. Neuberger et al.[21] presented the properties of graphene as promising features for the oil and gas industry applications.

Further, Yang et al. [22] reported the preparation process of magnetic graphene foam loaded with Fe_3O_4 nanoparticles, and showed that it was an excellent performance for the adsorption of organic solvents and oil. This computational research used the MD method to study the effect of GNS on hydraulic fracturing procedures. The MD method is a significant simulation that describes atomic behavior [23–28]. In our study, the GNS' affected on the hydraulic fracturing procedure with the MD method are studied first. Technically, for this purpose, we consider the effect of GNS edge, and atomic ratio on hydraulic fracturing procedure by reporting parameters like a mutual force between sand and rock particles, and the number of trapped sand particles in the rock matrix. In previous studies, hydraulic fracturing improvement in the presence of graphene nanostructures didn't report. So, we expected our results to be useful to optimize the natural hydraulic fracturing process and reducing extraction costs by increasing the efficiency of this procedure in the petroleum industry.

2. Computational method

The equilibrium MD simulation used in this computational study started at a temperature of 300 K. Technically, all simulations in our experiments used Large Scale Atomic Molecular Massively Simulator (LAMMPS) [29–32]. In defined models, the rock matrix was represented by atoms of O, Si, Al, Fe, Ca, Na, P, and Mg that were fixed in the MD box's lower area. But, for decreasing computational complexity, the sand particles were simulated using the coarse-grain technique, and this part of our MD simulation was considered sphere particles. Two rectangular gaps were created in the rock matrix to simulate atomic fracture in the rock matrix, as depicted in Fig. 2. Exactly, in the coarse-graining process of sand structure, each particle is represented as Si and O atoms. In these simulations, $\Delta t = 1$ was as the MD time step.

H_2O molecules and atomic sand structures filled the upper and middle sections of the simulation box. Fig. 3 shows the simulation box
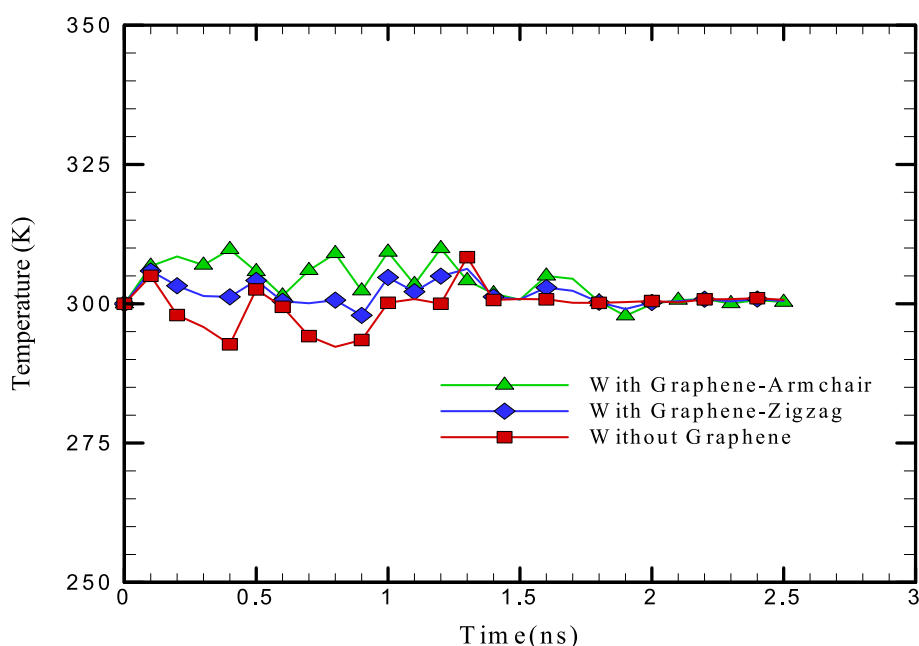
Fig. 4. Temperature changes of atomic structures without/with GNS in terms of MD simulation time.
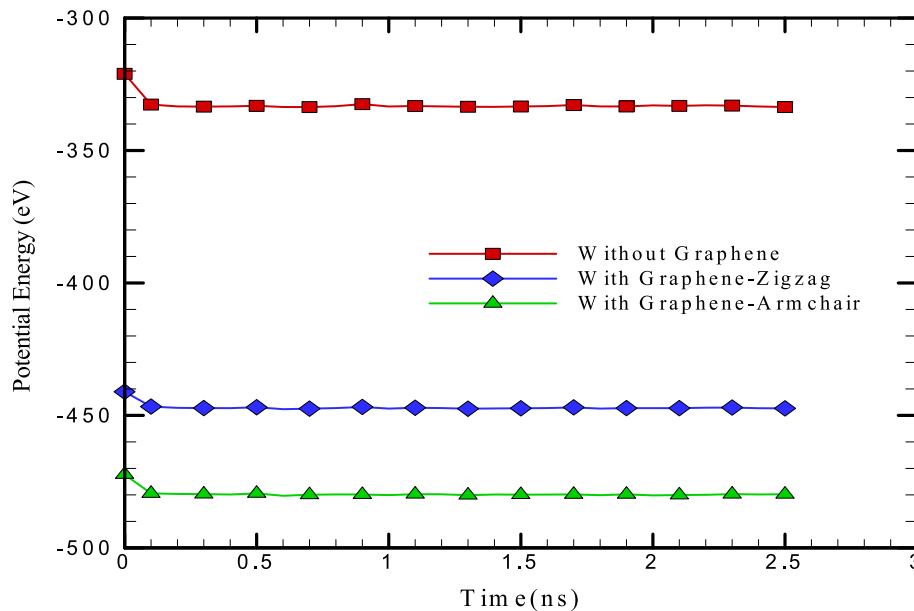
Fig. 5. Potential energy changes without/with GNS in terms of MD simulation time.

top, front, and perspective view [33]. Technically, the initial atomic structure generated by the Packmol software is shown in Fig. 3 [34]. Numerically, in the simulated structure, the NVT ensemble was implemented at 300 K in this ensemble, and the temperature damping factor of the structure was set to 0.01 [26]. The simulated structure was equilibrated after 2.5 ns at the initial temperature. NVT ensemble was then converted to an NVE ensemble hydraulic burst process simulation.

The atomic force field is an important factor in MD simulations. Using a coarse-grained model, a UFF was used in this computational study to simulate rock matrices and sand particle [35]. The Lennard-Jones (LJ) equation was computationally used to describe the potential energy of atomic structures in this force field. Interactions among atomic structures are loosely represented by the LJ equation. This equation was mentioned by John Lennard-Jones and stated as below [36]:

$$U_{LJ} = 4\varepsilon_{ij} \left[\left(\frac{\sigma_{ij}}{r} \right)^{12} - \left(\frac{\sigma_{ij}}{r} \right)^6 \right] \tag{1}$$

where, σ_{ij} is the distance, ε_{ij} is the depth of potential well, r_{ij} is the distance between two atoms. Table 1 shows the energy and length scale parameters for various atoms [35].

Bond strength and bond angular curvature factors are included in bonded interactions in the MD simulation. A simple harmonic oscillation form is used to estimate the bond strength and angular extension in the UFF. SPC model, which includes three atomic sites for electrostatic interactions and positive charges on H atoms, was used to describe H_2O molecules [37,38]. Furthermore, the Tersoff potential was applied to characterize graphene nanoparticles [39,40]. In this force field, the possible energies for the distribution of atoms are described by the distance component of atomic interactions. Tersoff potential is expressed by Eqs. (2) and (3):

$$E = \frac{1}{2} \sum_i \sum_{i \neq j} U_{ij} \tag{2}$$

$$U_{ij} = f_C(r_{ij}) \left[a_{ij} f_R(r_{ij}) + b_{ij} f_A(r_{ij}) \right] \tag{3}$$

where, $f_A(r_{ij})$ it includes three-body interactions and $f_R(r_{ij})$ is a two-body term. After identifying the proper force field to atomic structures, MD simulations were done. To calculate the displacement of atoms, Newton's second law represent as follows,

$$F_i = \sum_{i \neq j} F_{ij} = m_i \frac{d^2 r_i}{dt^2} = m_i \frac{dv_i}{dt} \tag{4}$$

From this equation and defining atomic force-field in our simulation, the velocity and position of various atoms in the MD simulation box were calculated using various integration processes, such as velocity-Verlet algorithm [41,42]. This computational procedure described the atomic evolution of simulated structures, and showed the final state in the defined time. MD simulations were performed in two main phases. Firstly, GNS and rock matrix with H_2O/sand fluid were simulated at T = 300 K for 2.5 ns. The simulation box size was $100 \times 50 \times 75$ Å^3. In this equilibration process, we used an NVT ensemble with 1 fs time step [43,44]. In the initial phase, the simulation process was verified by measuring the temperature and total energy of the simulated structures, and the time evolution of the atomic matrix and H_2O/sand fluid was then performed for 2.5 ns. In this step, the parameters like the number of sand particles and mutual atomic force trapped in rock matrix fracture were recorded. MD simulations details for described two phases reported in Table 2.

3. Results and discussion

3.1. Equilibration procedure of atomic structures

The equilibrium process is a crucial step in MD simulations that demonstrates the atomic stability of structures under certain circumstances. The atomic structure of rock matrix, and mixed fluid equilibrated at T = 300 K in the first stage. Temperature changes of atomic structures is shown in Fig. 4. Moreover, Fig. 5 shows the total energy of
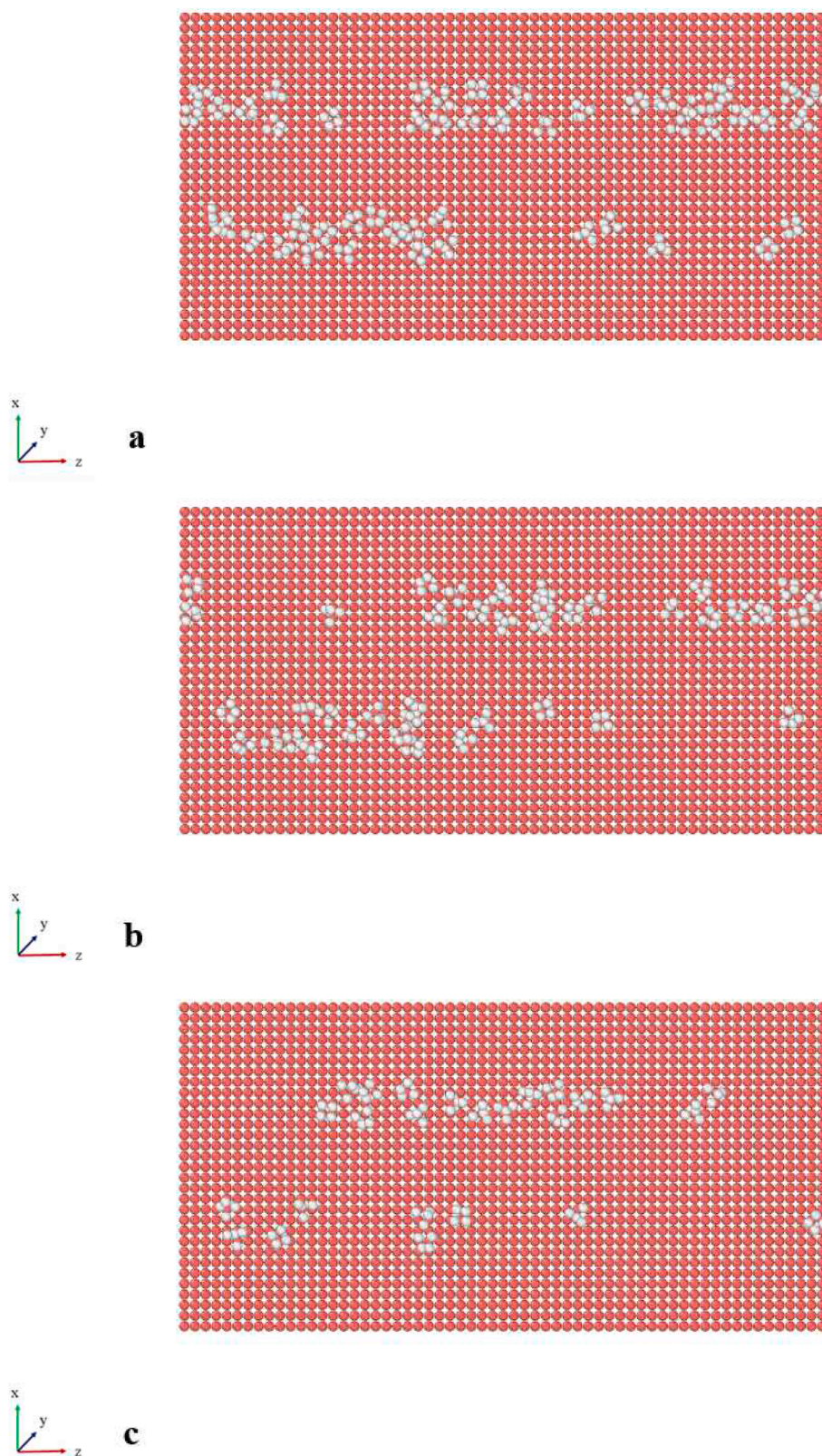
Fig. 6. Time evolution of sand removing from rock matrix after a) 0, b) 1 ns, c) 2.5 ns.
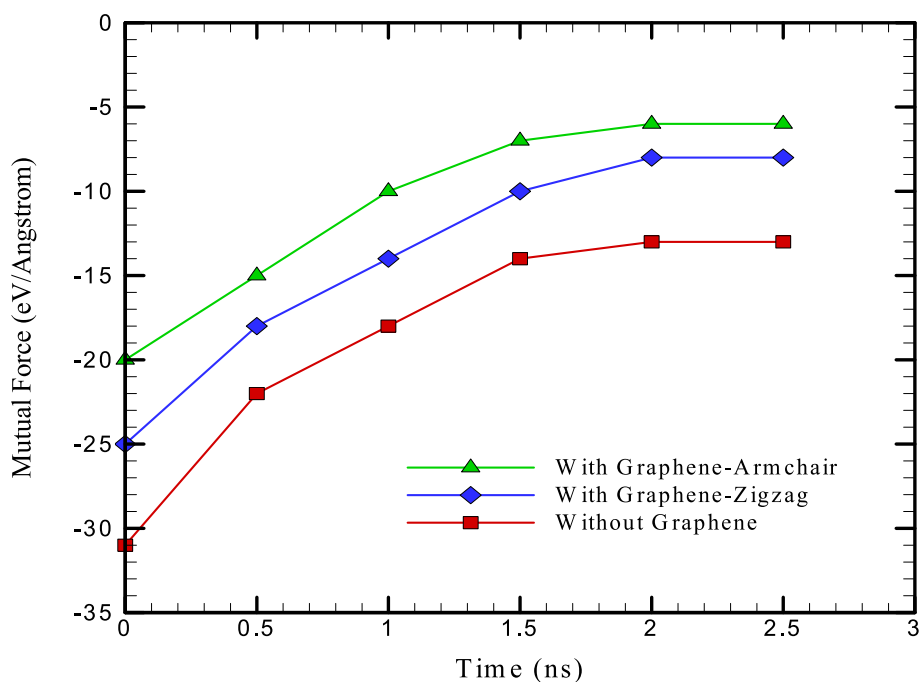
Fig. 7. Mutual force changes of rock matrix and sand particle mutual force without/with GNS in terms of simulation time.

Table 3
Mutual force difference of rock matrix and sand particle without/with graphene nanosheets after 2.5 ns.

Atomic Sample	Mutual Force (eV/Å)
Without GNS	−13
With armchair GNS	−6
With zig-zag GNS	−8

of structures. So, atomic distance increasing caused the potential energy, and total energy decreased. Finally, by decreasing these two energies, the simulated structure's stability decreased.

Additionally, adding GNS to initial mixture fluid enhanced the atomic stability of these structures. The total energy of these atomic structures converged from −333 eV to −447 eV and −479 eV, respectively, when zig-zag and armchair GNS were added to initial mixture fluid. These calculations show the physical convergence in the atomic evolution of simulated structures. Computationally, these numerical convergences arise from proper selecting of interatomic force-field and atomic arrangement in the simulated samples. In other words, the atomic arrangement of target samples adopted with defined force-field by MD time passing. So, physical stability of structures can be

structures based on simulation time. Based on this figure, we conclude the kinetic and potential energies of structures converged after 2.5 ns, and reached −333 eV. Theoretically, total energy directly related to potential energy and a reciprocal relationship with the atomic distance
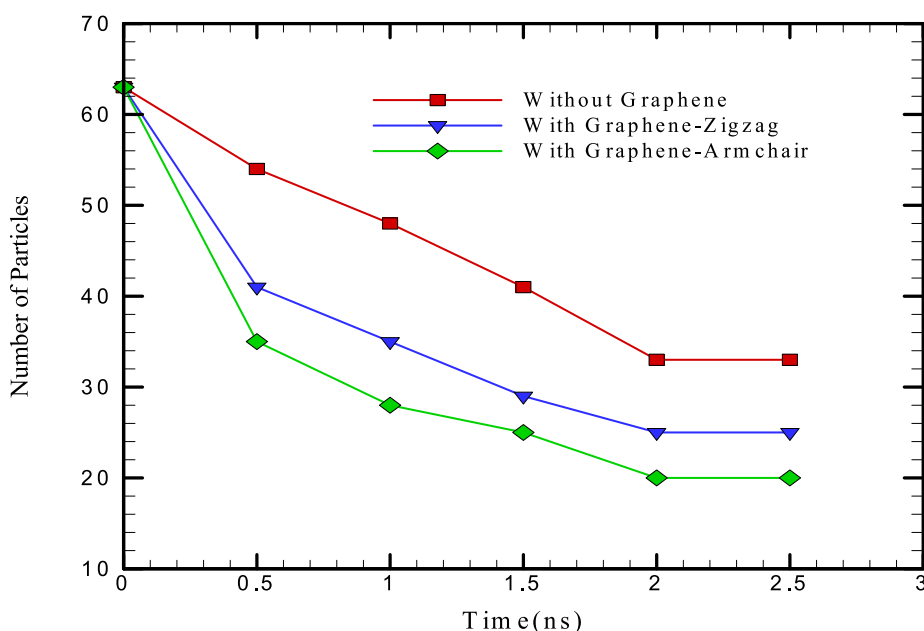
Fig. 8. Number of trapped sand particles in rock matrix without/with GNS in terms of simulation time.
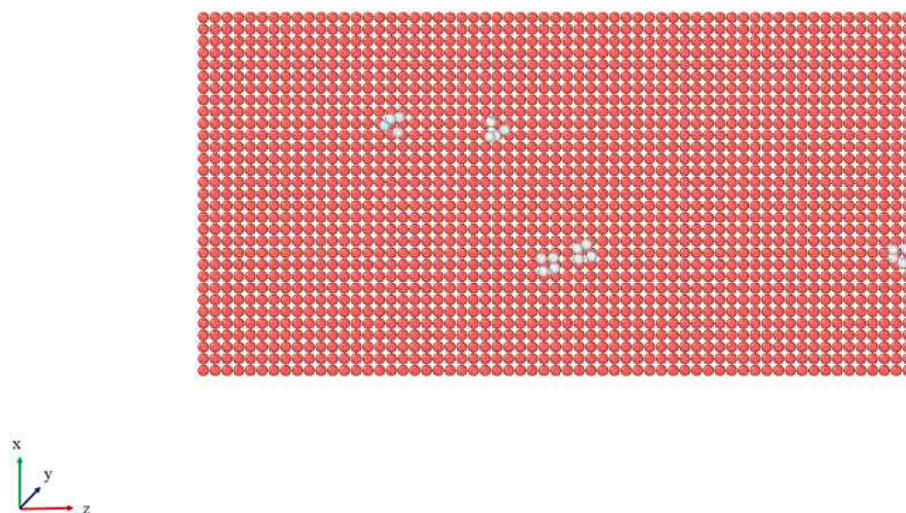
Fig. 9. Number of trapped sand particles in the rock matrix after 2.5 ns in the presence of armchair GNS.

Table 4
The number of trapped sand particles in the rock matrix without/with GNS after 2.5 ns.

Atomic Sample	Number of Trapped Particles
Without GNS	33
With armchair GNS	20
With zig-zag GNS	25

detected at standard condition. So, this process (temperature/potential energy convergence) validated our simulation method as reported in previous studies [45,46].

3.2. Dynamical evolution in simulated structures

NVT ensemble converted to NVE one for 2.5 ns after the process of equilibration. Fig. 6 depicts the time evolution of atomic structures in this ensemble. The mutual force among these atomic structures reduced from −31 to −13 eV/ Å, as seen in Fig. 7. The non-zero rate of mutual force rate showed the sand particle and rock matrix atomic distance was less, so we conclude these structures interacted with each other. The rock matrix attracted and trapped sand nanoparticles. These atomic phenomena had a disrupting effect in the petroleum industry and should be omitted. Numerically, based on Table 3, the mutual force decreased from −13 to −8, and −6 eV/Å by adding zig-zag and armchair GNS. Furthermore, Fig. 6 showed by simulation time passing, the mutual force between matrix and sand particles decreasing in presence of nano-structures and energy barriers ratio enlarging. This time evolution pre-dicted lesser number of sand particles diffused to atomic surface.

The number of trapped sand particles in rock matrix fracture was proportional to its stability. This computer study showed a reduction in trapped sand particles (Figs 8 and 9). After 2.5 ns, the number of trapped sand particle numerically decreased to 33. Based on Table 4, adding zigzag and armrest GNS to initial mixture increased the atomic fraction deviation to 74 and 63, respectively.

Then, we describe this atomic method. In this section, armchair GNS with an atomic ratio of 10%, 5%, 2.5% and 1% were introduced into the H$_2$O/sand mixture, and the number of sand particle trapped in the atom

matrix reported deaths (Fig. 10). Based on Fig. 11 and Table 5, the 2.5% GNS were able to detect the smallest amount of sand particles trapped in the original mixed liquid. Using GNS, the number of sand particles trapped in the rock matrix reaches 20, 14, 18, and 19, respectively.

This step reported the distance between the simulated matrix's center of Mass (COM) and H$_2$O/sand fluid. In these calculations, COM parameter showed the separation of atomic fluid from the initial matrix. MD simulations showed after 2.5 ns, the fluid and matrix COM varied from 3.57 Å to 10.24 Å (as depicted in Fig. 12). This atomic evolution indicated sand particles departed from the pristine matrix. Computa-tionally, 10.24 Å was the lesser cut-off radius in this simulations. This subject shows the negligible interaction between sand particles and atomic matrix as reported in the previous calculation (mutual force calculation).

Furthermore, sand particle volume calculation in the vicinity of atomic matrix showed GNS's effect on the sand departing process. As reported in Table 6, this physical parameter varied from 5321 to 278 Å^3 by time evolution from t = 0 to 2.5 ns. Physically, decreasing sand volume in the vicinity of the atomic matrix showed the improvement of fracturing process in the MD box. The stated atomic behavior detected for GNS adding procedure by equal or lesser than 10% atomic ratio. By GNS adding with larger ratio, the uniform distribution of nanoparticles was impossible, and fracturing process efficiency decreased. So, we can conclude the GNS adding by 10% value (optimized value), the fracturing process reached maximum efficiency. But, using more GNS (more than 10% ratio), the aggregation phenomenon detected in the MD box and departing sand particles from the atomic matrix were disrupted. Furthermore, GNS are very expensive, for overcome to this problem and reduce the operation cost of our proposed case, graphene-coated sur-faces can be implemented at the common surfaces between rock struc-ture and H$_2$O-sand mixture. Furthermore, this proposed solution can prevent from aggregation process occur in GNS.

The diffusion coefficient is another important parameter that can describe the GNS effects on the efficiency of the hydraulic fracturing process. To calculate this parameter for H$_2$O-sand system, the diffusion of various atoms in all directions was supposed. Computationally, the diffusion coefficient, of atomic structures can be measured by the sys-tem's slop of mean-squared displacement (MSD). MSD parameter rep-resents with below equation [38]:

$$MSD = \langle |r(t) - r_0|\rangle^2 \tag{5}$$

Where, r(t) is the position of each atom at time t and r_0 is the initial position in the simulated structure. Computationally, the slope of MSD versus time was proportional to the diffusion coefficient. Table 7 shows the diffusion coefficient change of simulated H_2O-sand system in MD simulation box as a function of GNS ratio. Numerically, by GNS ratio reached to 10%, the diffusion coefficient of simulated structures converged to $45.52 \times 10^{-8} cm^2.s^{-1}$ value. These results indicated the nanosheets cause more H_2O molecules to diffuse among sand particles. This atomic evolution occurred, more sand particles can be displaced with H_2O molecules in the hydraulic fracturing process.

The final section of this computational work calculated the interaction energy between rock substrate and H_2O-sand mixture. The simple/angular term of interaction energy listed in Table 8. The results show that the interaction energy between substrate and mixture converged to lesser values by armchair GNS inserting into the pristine mixture. This behavior resulted from the components' growing atomic distances, which increased the process's efficiency. Numerically, GNS inserting into H_2O-sand mixture caused interaction energy to converge to –32.38 eV for atomic systems at T = 300 K. Physically, this atomic evolution corresponded to increasing atomic displacement amplitude. The radial distribution function, or g(r), in a system of particles (atoms and molecules) in statistical mechanics showed how density changes in relation to distance from a reference particle. The position of maximum specified particle distribution for this parameter within the computational box and the g(r) ratio. The highest g(r) and location of this parameter for numerous modeled samples were given in Table 9. MD results predicted by GNS ratio settings to 2.5%, the g(r) value decreased and moved to larger distances. Numerically, maximum value of g(r) parameter converged to 10.18 and position of this parameter fixed at 4.84 Å. By this atomic arrangement changes, the density of trapped sand particles changed as a function of GNS ratio. MD results predicted the density of trapped sand particles changed from 0.361 atom/$Å^3$ to 0.214 atom/$Å^3$ in the presence of GNS with various atomic ratio (see Table 9). These outputs predicted lesser sand particles trapped in pristine matrix and hydraulic fracturing process was effectively done.

4. Conclusion

This computational work studied the atomic interaction between H_2O/sand mixture fluid and rock matrix without/with graphene nanoparticles via MD simulations. Technically, Tersoff and UFF potential were used to mixture fluid/rock matrix and nanoparticle structures, respectively. In practical applications in the oil industry, increasing hydraulic fracturing process efficiency can significantly reduce production costs. To this end, we tried to come up with a practical solution by examining the effects of GNS during hydraulic fracturing. The effectiveness of hydraulic fracturing was enhanced in our suggested method by increasing the number of sand particles that were removed
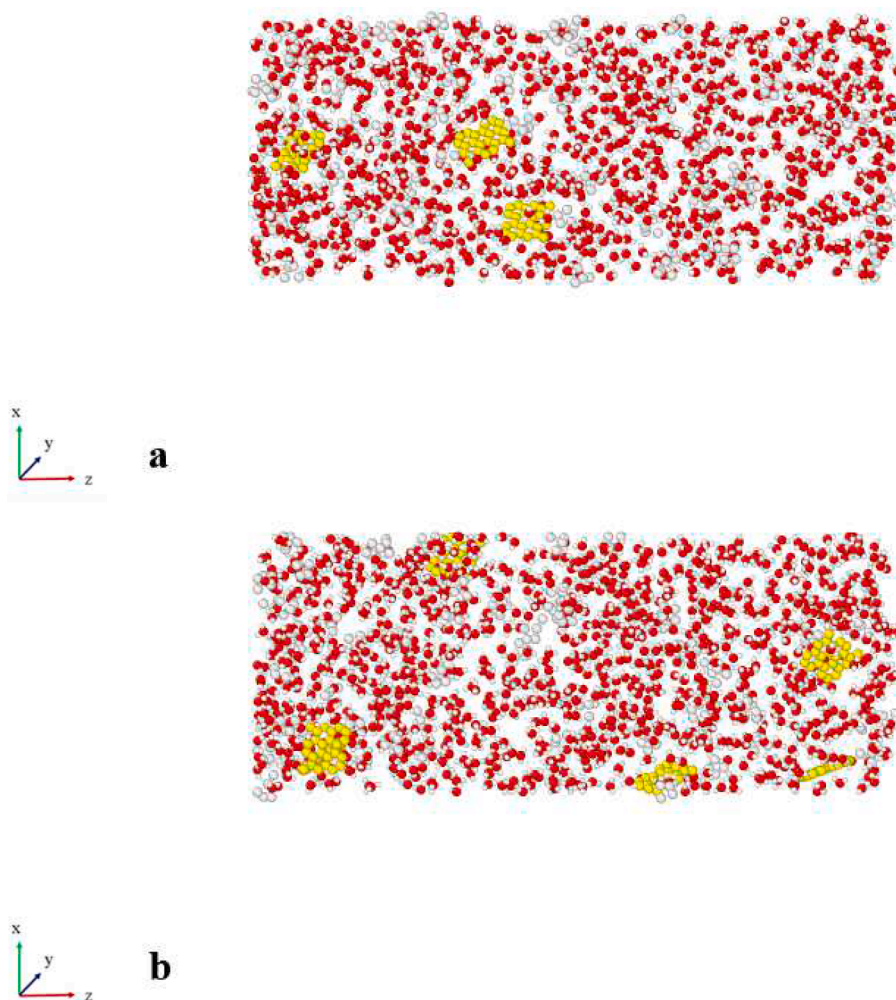
Fig. 10. H_2O/sand mixture fluid with: a) 1, b) 2.5, c) 5, and d) 10% GNS.
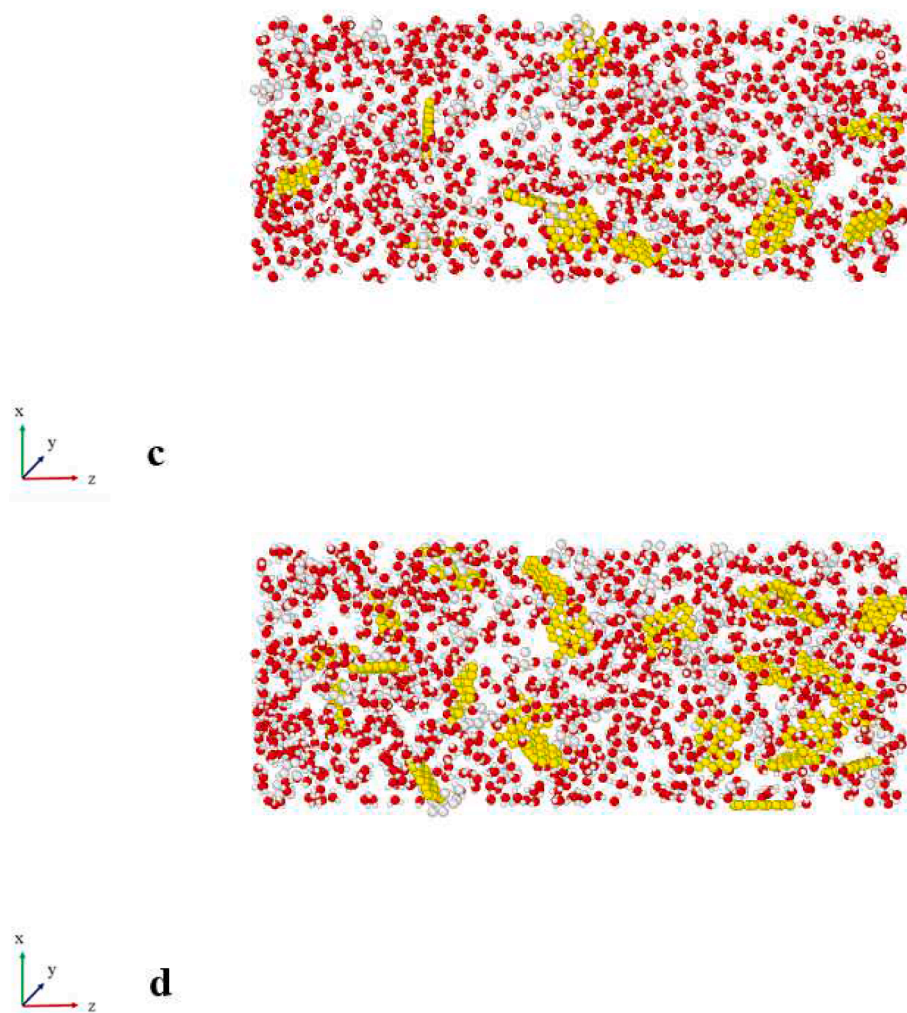
Fig. 10. (*continued*).
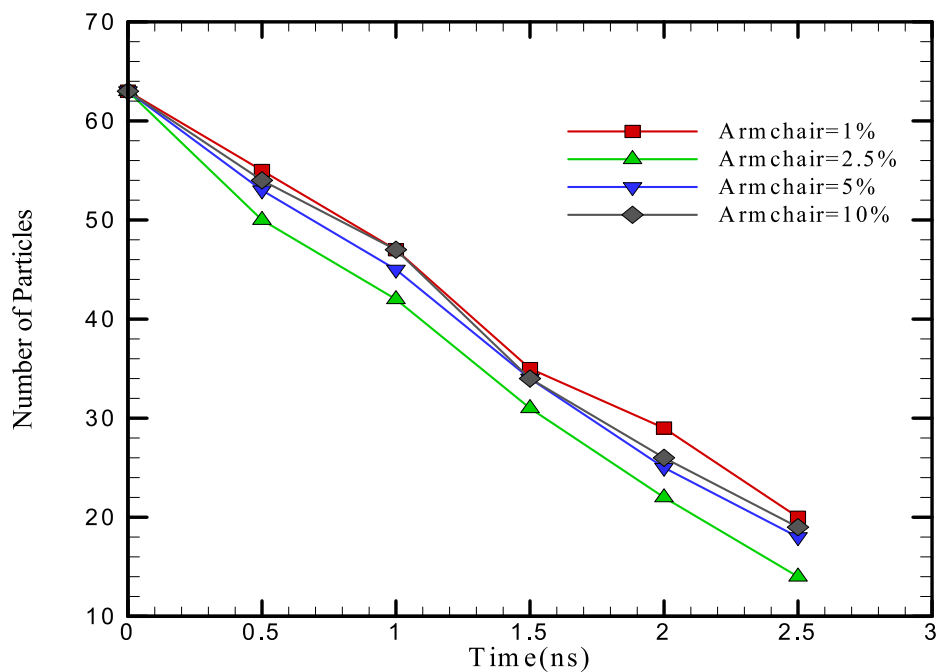
Fig. 11. The number of trapped sand particles in the rock matrix in terms of simulation time.

Table 5

The number of trapped sand particles according to GNS ratio after 2.5 ns.

GNS ratio (%)	Number of Trapped Particles
1	20
2.5	14
5	18
10	19

from the rock surface. Our computational findings demonstrated that GNS had a proper effect on the hydraulic fracturing process. So, our results from the MD simulation method are as following:

- The total energy converged to -479 and -333 eV after 2.5 ns without and with GNS.
- The mutual force between mixture fluid and rock matrix increases by GNS adding to initial fluid. The explained mutual force in these structures extended to numerically -6 and -13 eV/Å with and without GNS.
- The trapped sand particles in rock matrix fracture were decreased by GNS, inserting into the initial mixture fluid. The number of trapped particles decreased to 20 with 1% GNS ratio inserting into the MD simulation package.
- The diffusion coefficient of H_2O-sand mixture increases by GNS adding to MD box. Numerically, by 10% GNS ratio adding to the pristine mixture, diffusion coefficient in simulated structures reached $45.52 \times 10^{-8} cm^2.s^{-1}$.
- The interaction energy between H_2O-sand mixture and rock substrate decreased to -32.38 eV value by GNS adding to pristine mixture. By this evolution occur, more sand particles can be departed from the rock matrix.
- The maximum ratio of radial distribution function decreased to 10.18 and occurred in 4.84 Å by GNS ratio setting to 2.5%. This parameter outputs predicted high efficiency of hydraulic fracturing process in the presence of 2.5% GNS structure.

- The density of trapped sand particles decreased to 0.214 atom/$Å^3$ using GNS with optimum ratio.

CRediT authorship contribution statement

Wei Zhu: Methodology, Software, Validation. **Farahnaz Saberi:** Methodology, Software, Validation, Writing – original draft, Investigation. **S. Mohammad Sajadi:** Methodology, Software, Validation, Investigation. **Navid Nasajpour-Esfahani:** Methodology, Software, Validation, Writing – original draft, Investigation. **Maboud Hekmatifar:** Methodology, Software, Validation, Writing – original draft, Investigation. **As'ad Alizadeh:** Writing – original draft, Investigation. **D. Toghraie:** Writing – original draft, Investigation. **Roozbeh Sabetvand:** Writing – original draft, Investigation.

Declaration of Competing Interest

The authors declare that they have no known competing financial interests or personal relationships that could have appeared to influence the work reported in this paper.

Data availability

No data was used for the research described in the article.

Table 6

The number of trapped sand particles in the rock matrix in armchair GNS atomic ratio after 2.5 ns.

GNS ratio (%)	COM Distance(Å)	Volume($Å^3$)
1	6.55	530
2.5	7.54	412
5	8.71	324
10	10.24	278
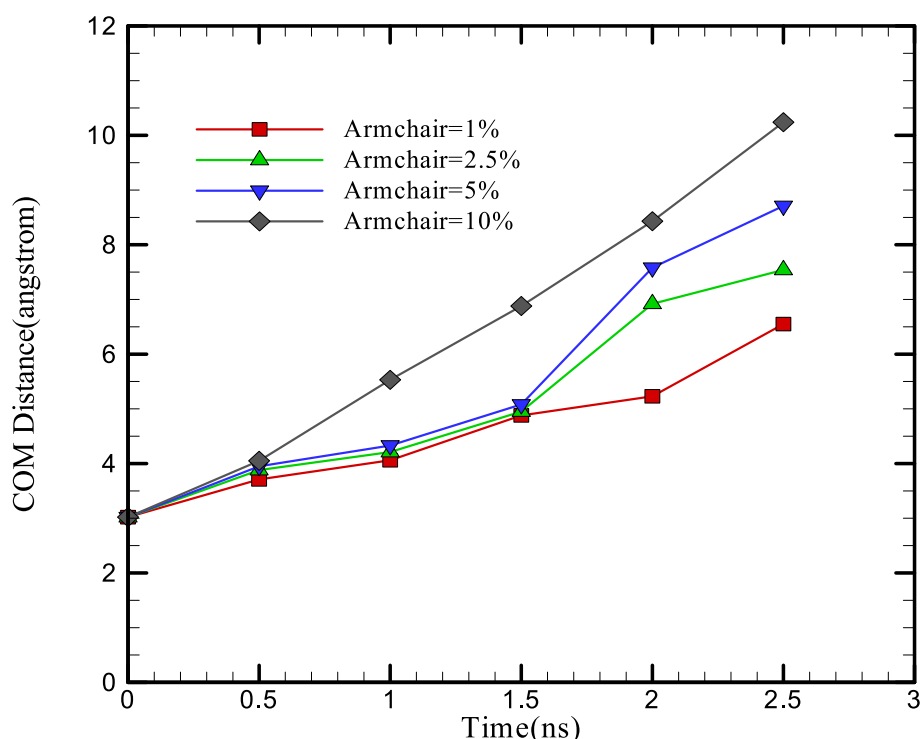
Fig. 12. The COM distance of matrix and sand particles in terms of simulation time.

Table 7

Diffusion coefficient of H$_2$O-sand system as a function of GNS ratio.

GNS ratio (%)	Diffusion Coefficient (10^{-8}cm^2.s^{-1})
1	33.41
2.5	38.79
5	43.07
10	45.52

Table 8

The interaction energy between rock substrate and H$_2$O-sand mixture as a function of armchair GNS ratio.

GNS Ratio (%)	Interaction Energy(eV)	
	Simple Term	Angle Term
1	−57.32	−11.29
2.5	−42.89	−10.55
5	−31.20	−8.37
10	−25.37	−7.01

Table 9

The value /position of maximum ratio of radial distribution function in modeled sand particles and density of trapped sands as a function of armchair GNS ratio after 2.5 ns.

GNS ratio (%)	g(r)	Distance(Å^3)	Density(atom/Å^3)
1	12.56	3.59	0.361
2.5	10.18	4.84	0.214
5	10.33	4.52	0.225
10	10.91	4.38	0.261

Acknowledgement

References

[1] L. Gandossi, and U. Von Estorff, "An overview of hydraulic fracturing and other formation stimulation technologies for shale gas production," *Eur. Commisison Jt. Res. Cent. Tech. Reports,* vol. 26347, 2013.

[2] T. Colborn, C. Kwiatkowski, K. Schultz, M. Bachran, Natural gas operations from a public health perspective, Hum. Ecol. Risk Assess. Int. J. 17 (5) (2011) 1039–1056.

[3] L.-B.-E.-E. Map, Methane in Pennsylvania water wells unrelated to Marcellus shale fracturing, Oil Gas J. (2011) 55.

[4] M. Hekmatifar, D. Toghraie, A. Khosravi, F. Saberi, F. Soltani, R. Sabetvand, A. S. Goldanlou, The study of asphaltene desorption from the iron surface with molecular dynamics method, J. Mol. Liq. 318 (2020), 114325.

[5] D. Blundell, N. Arndt, P.R. Cobbold, C. Heinrich, 9: Processes of tectonism, magmatism and mineralization: lessons from Europe, Ore Geol. Rev. 27 (1–4) (2005) 333–349.

[6] D.T. Allen, V.M. Torres, J. Thomas, D.W. Sullivan, M. Harrison, A. Hendler, S. C. Herndon, C.E. Kolb, M.P. Fraser, A.D. Hill, Measurements of methane emissions at natural gas production sites in the United States, Proc. Natl. Acad. Sci. 110 (44) (2013) 17768–17773.

[7] C.D. Kassotis, D.E. Tillitt, J.W. Davis, A.M. Hormann, S.C. Nagel, Estrogen and androgen receptor activities of hydraulic fracturing chemicals and surface and ground water in a drilling-dense region, Endocrinology 155 (3) (2014) 897–907.

[8] S. Chalupka, Occupational silica exposure in hydraulic fracturing, Workplace health & safety 60 (10) (2012).

[9] V. J. Brown, "Industry issues: Putting the heat on gas," National Institute of Environmental Health Sciences, 2007.

[10] V. J. Brown, "Radionuclides in fracking wastewater: managing a toxic blend," National Institute of Environmental Health Sciences, 2014.

[11] A.M. Bamber, S.H. Hasanali, A.S. Nair, S.M. Watkins, D.I. Vigil, M. Van Dyke, T. S. McMullin, K. Richardson, A systematic review of the epidemiologic literature assessing health outcomes in populations living near oil and natural gas operations: study quality and future recommendations, Int. J. Environ. Res. Public Health 16 (12) (2019) 2123.

[12] R. Wright, R.D. Muma, High-volume hydraulic fracturing and human health outcomes: a scoping review, J. Occup. Environ. Med. 60 (5) (2018) 424–429.

[13] M. Wigwe, O. Kolawole, M. Watson, I. Ispas, and W. Li, "Influence of fracture treatment parameters on hydraulic fracturing optimization in unconventional formations.".

[14] A. Jahandideh, B. Jafarpour, Optimization of hydraulic fracturing design under spatially variable shale fracability, J. Pet. Sci. Eng. 138 (2016) 174–188.

[15] K. Cao, P. Siddhamshetty, Y. Ahn, R. Mukherjee, J.-S.-I. Kwon, Economic model-based controller design framework for hydraulic fracturing to optimize shale gas production and water usage, Ind. Eng. Chem. Res. 58 (27) (2019) 12097–12115.

[16] Chen, L., Zhao, Y., Li, M., Li, L., Hou, L.,... Hou, H. (2021). Reinforced AZ91D magnesium alloy with thixomolding process facilitated dispersion of graphene nanoplatelets and enhanced interfacial interactions. Materials Science and Engineering: A, 804, 140793. https://doi.org/10.1016/j.msea.2021.140793.

[17] Li, M., Guo, Q., Chen, L., Li, L., Hou, H.,... Zhao, Y. (2022). Microstructure and properties of graphene nanoplatelets reinforced AZ91D matrix composites prepared by electromagnetic stirring casting. Journal of Materials Research and Technology, 21, 4138-4150. https://doi.org/10.1016/j.jmrt.2022.11.033.

[18] L. Chen, Y. Zhao, J. Jing, H. Hou, Microstructural evolution in graphene nanoplatelets reinforced magnesium matrix composites fabricated through thixomolding process, J. Alloy. Compd. 940 (2023), 168824, https://doi.org/10.1016/j.jallcom.2023.168824.

[19] S. Tian, N.I. Arshad, D. Toghraie, S.A. Eftekhari, M. Hekmatifar, Using perceptron feed-forward Artificial Neural Network (ANN) for predicting the thermal conductivity of graphene oxide-Al2O3/water-ethylene glycol hybrid nanofluid, Case Studies in Thermal Eng. 26 (2021), 101055.

[20] A. Sepehri, M. K. G. Al-askari, and A. Heydari, "Graphene Plays a Role as a Magic Material for Revolution in the Petroleum Industry," *Available at SSRN 3254158*, 2018.

[21] N. Neuberger, H. Adidharma, M. Fan, Graphene: a review of applications in the petroleum industry, J. Pet. Sci. Eng. 167 (2018) 152–159.

[22] S. Yang, L. Chen, L. Mu, P.-C. Ma, Magnetic graphene foam for efficient adsorption of oil and organic solvents, J. Colloid Interface Sci. 430 (2014) 337–344.

[23] Zhang, L., Xiong, D., Su, Z., Li, J., Yin, L., Yao, Z.,... Zhang, H. (2022). Molecular dynamics simulation and experimental study of tin growth in SAC lead-free microsolder joints under thermo-mechanical-electrical coupling. Materials Today Communications, 33, 104301. 10.1016/j.mtcomm.2022.104301.

[24] S. Gao, H. Wang, H. Huang, R. Kang, Molecular simulation of the plastic deformation and crack formation in single grit grinding of 4H-SiC single crystal, Int. J. Mech. Sci. 247 (2023), 108147, https://doi.org/10.1016/j.ijmecsci.2023.108147.

[25] N.A. Jolfaei, N.A. Jolfaei, M. Hekmatifar, A. Piranfar, D. Toghraie, R. Sabetvand, S. Rostami, Investigation of thermal properties of DNA structure with precise atomic arrangement via equilibrium and non-equilibrium molecular dynamics approaches, Comput. Methods Programs Biomed. 185 (2020), 105169.

[26] A.Z. Ashkezari, N.A. Jolfaei, N.A. Jolfaei, M. Hekmatifar, D. Toghraie, R. Sabetvand, S. Rostami, Calculation of the thermal conductivity of human serum albumin (HSA) with equilibrium/non-equilibrium molecular dynamics approaches, Comput. Methods Programs Biomed. 188 (2020), 105256.

[27] A. Asgari, Q. Nguyen, A. Karimipour, Q.-V. Bach, M. Hekmatifar, R. Sabetvand, Develop molecular dynamics method to simulate the flow and thermal domains of H 2 O/Cu nanofluid in a nanochannel affected by an external electric field, Int. J. Thermophys. 41 (9) (2020) 1–14.

[28] Y. Zheng, X. Zhang, M.T.S. Mobareke, M. Hekmatifar, A. Karimipour, R. Sabetvand, Potential energy and atomic stability of H2O/CuO nanoparticles flow and heat transfer in non-ideal microchannel via molecular dynamic approach: the green–Kubo method, J. Therm. Anal. Calorim. 144 (6) (2021) 2515–2523.

[29] S. Plimpton, Fast parallel algorithms for short-range molecular dynamics, J. Comput. Phys. 117 (1) (1995) 1–19.

[30] W.M. Brown, P. Wang, S.J. Plimpton, A.N. Tharrington, Implementing molecular dynamics on hybrid high performance computers–short range forces, Comput. Phys. Commun. 182 (4) (2011) 898–911.

[31] W.M. Brown, A. Kohlmeyer, S.J. Plimpton, A.N. Tharrington, Implementing molecular dynamics on hybrid high performance computers–Particle–particle particle-mesh, Comput. Phys. Commun. 183 (3) (2012) 449–459.

[32] R.M. Mukherjee, P.S. Crozier, S.J. Plimpton, K.S. Anderson, Substructured molecular dynamics using multibody dynamics algorithms, Int. J. Non Linear Mech. 43 (10) (2008) 1040–1055.

[33] A. Stukowski, Visualization and analysis of atomistic simulation data with OVITO–the open visualization tool, Model. Simul. Mater. Sci. Eng. 18 (1) (2009), 015012.

[34] L. Martínez, R. Andrade, E.G. Birgin, J.M. Martínez, PACKMOL: a package for building initial configurations for molecular dynamics simulations, J. Comput. Chem. 30 (13) (2009) 2157–2164.

[35] A.K. Rappé, C.J. Casewit, K. Colwell, W.A. Goddard III, W.M. Skiff, UFF, a full periodic table force field for molecular mechanics and molecular dynamics simulations, J. Am. Chem. Soc. 114 (25) (1992) 10024–10035.

[36] J. E. Jones, "On the determination of molecular fields.—II. From the equation of state of a gas," *Proceedings of the Royal Society of London. Series A, Containing Papers of a Mathematical and Physical Character,* vol. 106, no. 738, pp. 463-477, 1924.

[37] K. Toukan, A. Rahman, Molecular-dynamics study of atomic motions in water, Phys. Rev. B 31 (5) (1985) 2643.

[38] H. Berendsen, J. Grigera, T. Straatsma, The missing term in effective pair potentials, J. Phys. Chem. 91 (24) (1987) 6269–6271.

[39] J. Tersoff, Modeling solid-state chemistry: Interatomic potentials for multicomponent systems, Phys. Rev. B 39 (8) (1989) 5566.

[40] J. Tersoff, New empirical approach for the structure and energy of covalent systems, Phys. Rev. B 37 (12) (1988) 6991.

[41] L. Verlet, Computer" experiments" on classical fluids. I. thermodynamical properties of Lennard-Jones molecules, Phys. Rev. 159 (1) (1967) 98.

[42] W. Press, S. Teukolsky, W. Vetterling, B. Flannery, Section 17.4. second-order conservative equations. Numerical Recipes: The Art of Scientific Computing, 3rd ed.,, Cambridge University Press, New York, 2007.

[43] S. Nosé, A unified formulation of the constant temperature molecular dynamics methods, J. Chem. Phys. 81 (1) (1984) 511–519.

[44] W.G. Hoover, Canonical dynamics: equilibrium phase-space distributions, Phys. Rev. A 31 (3) (1985) 1695.

[45] A. Asgari, Q. Nguyen, A. Karimipour, Q.-V. Bach, M. Hekmatifar, R. Sabetvand, Investigation of additives nanoparticles and sphere barriers effects on the fluid flow inside a nanochannel impressed by an extrinsic electric field: a molecular dynamics simulation, J. Mol. Liq. (2020), 114023.

[46] Karimipour, A., Jolfaei, N. A., Hekmatifar, M., Toghraie, D., Sabetvand, R., & Karimipour, A. (. Prediction of the interaction between HIV viruses and Human Serum Albumin (HSA) molecules using an equilibrium dynamics simulation program for application in bio medical science. Journal of Molecular Liquids, 113989, 2020.